

# A Robust Approach to Dynamic Feedback Linearization

Edgar Ergueta\* and Roberto Horowitz†

*Department of Mechanical Engineering,  
University of California, Berkeley, CA 94720*

Robert Seifried‡

*Institute of Engineering and Computational Mechanics  
University of Stuttgart, 70550 Stuttgart, Germany*

(Dated: March 19, 2009)

## Abstract

This paper presents two different control strategies for paper position control in printing devices. The first strategy is based on standard feedback linearization plus dynamic extension (dynamic feedback linearization). Even though this controller is very simple to design, we show that it is not able to handle actuator multiplicative uncertainties, and therefore it fails when it is implemented on the experimental setup. The second strategy we present uses similar concepts, but it is more robust since feedback linearization is used only to linearize the kinematics of the system and internal loops are used to locally control the actuator's positions and velocities. In this paper not only do we formally prove the robustness of the second control strategy, but we also show its successful implementation.

PACS numbers:

---

\*Electronic address: [Edgar.Ergueta@wdc.com](mailto:Edgar.Ergueta@wdc.com)

†Electronic address: [horowitz@me.berkeley.edu](mailto:horowitz@me.berkeley.edu)

‡Electronic address: [seifried@itm.uni-stuttgart.de](mailto:seifried@itm.uni-stuttgart.de)

## I. INTRODUCTION

Static feedback linearization is a nonlinear technique widely used for the control of MIMO nonlinear systems. As explained in [1] and [2], it consists in differentiating each of the outputs several times until at least one of the inputs appears. At that point we obtain a decoupling matrix, which needs to be inverted in order to linearize the system. Once the system is linearized through this transformation, pole placement is used to achieve the desired control objective. Unfortunately, sometimes this decoupling matrix is singular, making static feedback linearization fail.

A common solution to this problem, usually referred as dynamic feedback linearization, has been presented in [1], [2], [3], and [4]. Such a solution consists on adding integrators to some of the input channels in order to delay the appearance of the inputs when differentiating the outputs. Proceeding in this way, it might be possible to construct a new non-singular decoupling matrix. However, even if we succeed in finding an invertible decoupling matrix, the control strategy can be very sensible to model parameter uncertainties. For such cases, it is sometimes advised to modify this standard technique in order to gain in robustness.

In particular, in this paper we show how a *Dynamic Feedback Linearization* controller cannot be directly implemented in a mechatronic application for paper position control on printing devices, and a *Robust Feedback Linearization Plus Inner Loops* controller needs to be used instead. This controller has been presented in [5] and [6]; it uses feedback linearization to linearize only the kinematics of the system, and uses internal loops to locally control the actuators's positions and velocities.

The mechatronic application discussed in this paper has been presented in [7], [8] and [9]. The idea behind this mechanism is shown in Fig. 1 ([10]), and it consists on two steerable nips that permit the control of the longitudinal, lateral, and angular positions of a sheet, while it is being driven forward. As mentioned in [7] and [8], this mechanism resembles that of a two-wheel robot [11]; however, not only does the two-wheel robot have one less degree of freedom than the steerable nips system, but also the control law proposed by [11] fails to account for singularities that arise when the steering angle of the wheels approaches zero. Moreover, whereas the two-wheel robot requires three inputs to follow a reference trajectory, the steerable nips require four in order to steer and rotate each roller (see Fig. 1).

The asymptotic stability of the *Robust Feedback Linearization Plus Inner Loops* control

strategy has been already proved in [5] and [12]. Such stability analysis was conducted primarily to tune the control system gains in order to achieve a set of performance parameters, mainly to reduce tracking errors by a pre-specified amount in a finite specified time. However, we will now show its robustness to actuator multiplicative uncertainties by analyzing its convergence as time goes to infinity and seeking to attain exponential stability of the nominal system. Furthermore, we will contrast its robustness to that of the *Dynamic Feedback Linearization* controller.

The remainder of this paper is organized as follows. Section II describes the steerable nips mechanism and presents its model. Section III presents the development of the *Dynamic Feedback Linearization* controller designed for this application, and Section IV presents the *Robust Feedback Linearization Plus Inner Loops* controller, which has been successfully implemented on the experimental setup. Section V compares the robustness of both control strategies and Section VI presents experimental results. Finally, some concluding remarks are stated in Section VII.

## II. STEERABLE NIPS MECHANISM

As mentioned in Section I, the idea behind the steerable nips mechanism is shown in Fig. 1. Specifically, this figure shows a sheet moving along a flat surface through the steerable nips mechanism, and in the direction of the arrow labeled  $\underline{v}$ . This mechanism has been designed so that it can correct for lateral sheet position errors without having to translate any actuators and without inflicting any damage on the paper. This is possible by steering the two rollers shown in the figure, which are underneath a backer ball. As a result, each roller is in contact with the sheet at only one point, letting the sheets safely move laterally while they are being driven forward. The roller is driven by a servo motor (*process direction motor*) attached to a rotating table, which is in turn steered by another servo motor (*steering motor*). A complete description of this mechanism can be found in [8] and [9]. Note that in Fig. 1, the two rollers, located at points 1 and 2, are separated by a fixed distance  $2b$ .

In [5] and [13] we were able to show asymptotic convergence of the *Robust Feedback Linearization Plus Inner Loops* control strategy (described in Section IV) only for a sheet of finite length and thus, for finite time. Such constraints were necessary because one of the control objectives was that the sheet's leading edge needed to track a desired reference, which

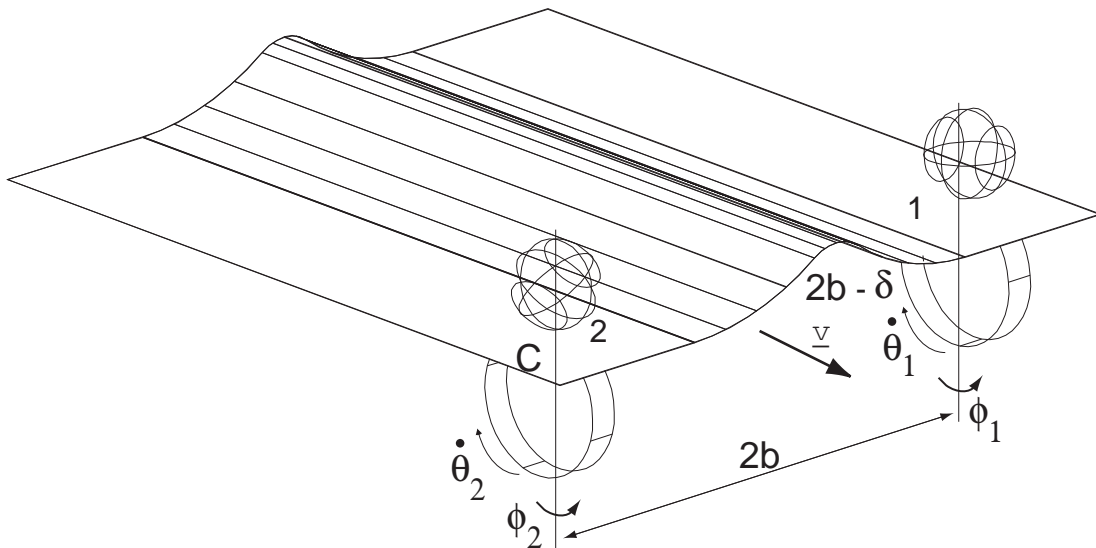


FIG. 1: Steerable nips with paper buckle

moved at a constant speed. In practice, however, sheets have finite length and therefore, the leading edge of the sheet only needs to be controlled until it reaches the beginning of the Image Transfer Station (ITS). By maintaining this control architecture, as time goes to infinity, so does the length of the page, and the control effort to control the position of the leading edge of the sheet becomes increasingly larger. Thus, in order to conduct a robustness analysis, we will require that the sheet track a constant longitudinal speed in the longitudinal direction instead of requiring that the position of the leading edge of the paper track a reference position trajectory moving with a constant speed. As will be shown in Section V A, by imposing velocity rather than position control, in the longitudinal direction, the tracking errors in the nominal system converge exponentially rather than just asymptotically since we no longer require to control the position of the leading edge of a sheet whose length goes to infinity.

Furthermore, in [5] and [13] we used the leading right corner of the sheet (point  $C$  in Fig. 1) as a reference for controlling the lateral and longitudinal positions of the page. However, since we will consider a page of infinite length, we would like to completely decouple lateral from longitudinal positions as in Fig. 2. Specifically, we will refer to the lateral position of the page,  $x$ , as the point along the lateral edge of the sheet that is in contact with the lateral sensor shown in this figure. Similarly, we will define the longitudinal position of the sheet,

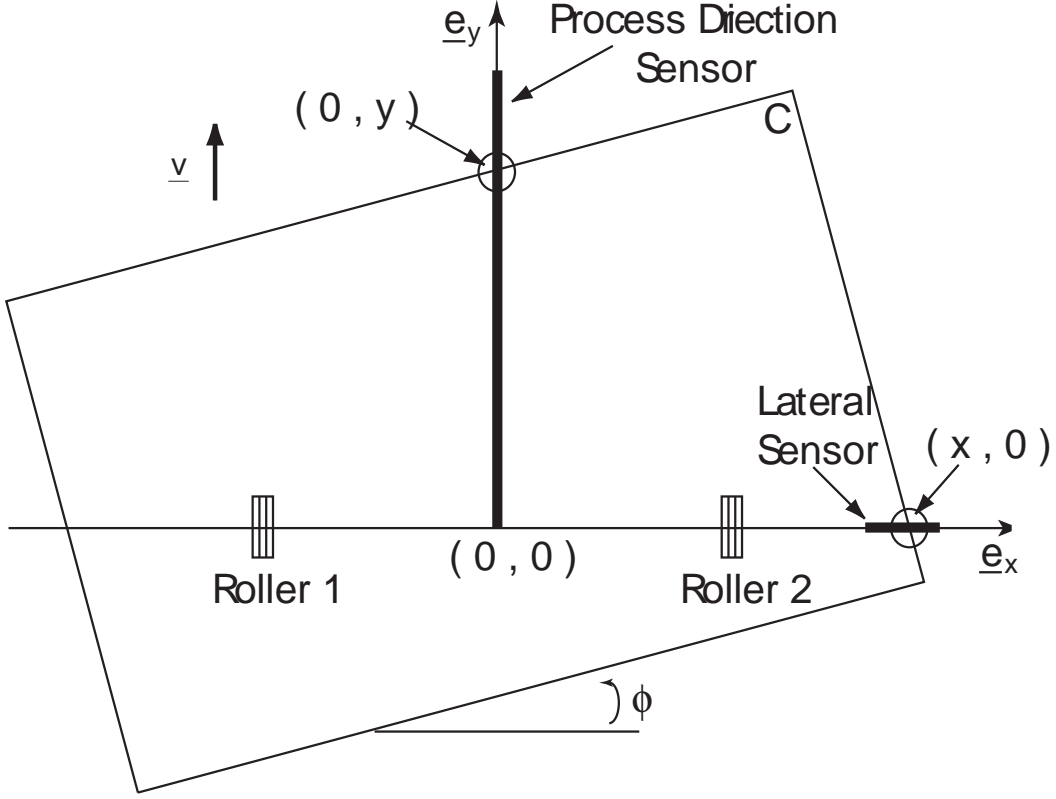


FIG. 2: Top view of steerable nips

$y$ , as the point along the leading edge of the sheet that is in contact with the longitudinal sensor located along the process direction in the middle of rollers 1 and 2;  $\phi$  will represent the angular position of the sheet. Note that since the two rollers steer independently, the sheet can also buckle or stretch. Thus we need to keep buckling at a minimum and make sure that the sheet never stretches. As shown in Fig. 1, we define the amount of buckling of the sheet,  $\delta$ , as the difference between the distance separating points 1 and 2 as measured along the paper ( $2b - \delta$ ) and along a straight line ( $2b$ ). Furthermore,  $\dot{\theta}_i$  ( $i = 1, 2$ ) represents the angular velocity of the rollers in the direction parallel to the sheet, and  $\phi_i$  ( $i = 1, 2$ ) represents their angular position in the direction perpendicular to the sheet.

The steerable nips mechanism has four nonholonomic constraints, which come from non-slip conditions on the rollers and local velocities (of the paper) being zero in the direction perpendicular to the rotation of the rollers at the point of contact with the rollers. Thus, its kinematics model is derived so that these constraints are satisfied at all times; they are

represented by the following equations:

$$\begin{aligned}
\dot{x} &= r_2 \dot{\theta}_2 (\sin \phi_2 - \frac{x+b}{2b} \tan \phi \cos \phi_2) \\
&\quad + r_1 \dot{\theta}_1 \frac{x-b}{2b} \tan \phi \cos \phi_1 := f_x(\underline{x}) \\
\dot{y} &= -r_2 \dot{\theta}_2 (\sin \phi_2 \tan \phi + \frac{y \tan \phi + b}{2b} \cos \phi_2) \\
&\quad + r_1 \dot{\theta}_1 \frac{y \tan \phi - b}{2b} \cos \phi_1 := f_y(\underline{x}) \\
\dot{\phi} &= \frac{1}{2b} (r_1 \cos \phi_1 \dot{\theta}_1 - r_2 \cos \phi_2 \dot{\theta}_2) := f_\phi(\underline{x}) \\
\dot{\delta} &= r_2 \sin \phi_2 \dot{\theta}_2 - r_1 \sin \phi_1 \dot{\theta}_1 := f_\delta(\underline{x})
\end{aligned} \tag{1}$$

where  $r_1$  and  $r_2$  are the radii of the two rollers, and the state vector is given by  $\underline{x} = [x \ \phi \ \delta \ \phi_1 \ \phi_2 \ \dot{\theta}_2 \ \dot{\theta}_1 \ \dot{\phi}_1 \ \dot{\phi}_2]^T$ . As mentioned in [8], a simple model that adequately describes both the process direction and steering actuator dynamics is given by

$$\begin{aligned}
\ddot{\theta}_i + \alpha_{pi} \dot{\theta}_i &= \beta_{pi} V_{pi}; \quad (i = 1, 2) \\
\ddot{\phi}_i + \alpha_{si} \dot{\phi}_i &= \beta_{si} V_{si}; \quad (i = 1, 2)
\end{aligned} \tag{2}$$

where  $V_{ji}$  is the input voltage to each motor, and  $\alpha_{ji}$  and  $\beta_{ji}$  are coefficients that depend on the inertias and rotational viscous damping coefficients of the different components of the steer-able nips mechanism. Subindexes  $p$  and  $s$  stand for process direction and steering actuators, respectively. Using Eqs. (1) and (2) we obtain the following state space representation:

$$\begin{aligned}
\frac{d}{dt} \begin{bmatrix} x \\ \phi \\ \delta \\ \phi_1 \\ \phi_2 \\ \dot{\theta}_1 \\ \dot{\theta}_2 \\ \dot{\phi}_1 \\ \dot{\phi}_2 \end{bmatrix} &= \begin{bmatrix} f_x(\underline{x}) \\ f_\phi(\underline{x}) \\ f_\delta(\underline{x}) \\ \dot{\phi}_1 \\ \dot{\phi}_2 \\ -\alpha_{p1} \dot{\theta}_1 \\ -\alpha_{p2} \dot{\theta}_2 \\ -\alpha_{s1} \dot{\phi}_1 \\ -\alpha_{s2} \dot{\phi}_2 \end{bmatrix} + \begin{bmatrix} 0 & 0 & 0 & 0 \\ 0 & 0 & 0 & 0 \\ 0 & 0 & 0 & 0 \\ 0 & 0 & 0 & 0 \\ 0 & 0 & 0 & 0 \\ \beta_{p1} & 0 & 0 & 0 \\ 0 & \beta_{p2} & 0 & 0 \\ 0 & 0 & \beta_{s1} & 0 \\ 0 & 0 & 0 & \beta_{s2} \end{bmatrix} \begin{bmatrix} V_{p1} \\ V_{p2} \\ V_{s1} \\ V_{s2} \end{bmatrix} \\
\underline{y} &= \begin{bmatrix} x \\ y_L \\ \phi \\ \delta \end{bmatrix}
\end{aligned} \tag{3}$$

where  $f_x(\underline{x})$ ,  $f_\phi(\underline{x})$ , and  $f_\delta(\underline{x})$  are defined in Eqs. (1), and  $\dot{y}_L$  is equal to  $f_y(\underline{x})$  evaluated at  $y = L$ .

### III. DYNAMIC FEEDBACK LINEARIZATION CONTROLLER

In this section we will first show that pure feedback linearization cannot be applied to the steerable nips system. Then, we will show that even though a strategy based on *Dynamic Feedback Linearization* can be designed, it cannot be implemented on the experimental setup due to actuator multiplicative uncertainties.

As mentioned in Section II, the control objective is to control the lateral and angular positions of the sheet before it arrives to the ITS as well as its velocity at that location. This needs to be accomplished within a finite pre-specified time and through the use of four control inputs. Two of these inputs rotate and steer one roller, and the other two inputs rotate and steer the other roller.

If we simply use static feedback linearization for this system, differentiating outputs  $x$ ,  $\phi$ , and  $\delta$  twice, and output  $\dot{y}_L$  once, we obtain an expression of the form

$$\begin{bmatrix} \ddot{x} & \ddot{y}_L & \ddot{\phi} & \ddot{\delta} \end{bmatrix}^T = A(\underline{x}) + B(\underline{x}) \begin{bmatrix} V_{p1} & V_{p2} & V_{s1} & V_{s2} \end{bmatrix}^T \quad (4)$$

where the decoupling matrix  $B(\underline{x})$  is singular. Thus, following the work presented in [1], [2], [3], and [4], in order to obtain a new nonsingular decoupling matrix, we add an integrator to the input channels corresponding to  $V_{p1}$  and  $V_{p2}$ . Proceeding in this way,  $V_{p1}$  and  $V_{p2}$  become new states of the system and their derivatives become two of the control inputs. We then define the new states  $z_i$  ( $i = 1, 2$ ) and new control inputs  $w_i$  ( $i=1-4$ ) as

$$\begin{aligned} z_1 &= V_{p1}; & \dot{z}_1 &= w_1 \\ z_2 &= V_{p2}; & \dot{z}_2 &= w_2 \\ w_3 &= V_{s1}; & w_4 &= V_{s2} \end{aligned} \quad (5)$$

and obtain the following enlarged system:

$$\frac{d}{dt} \begin{bmatrix} x \\ \phi \\ \delta \\ \phi_1 \\ \phi_2 \\ \dot{\theta}_1 \\ \dot{\theta}_2 \\ \dot{\phi}_1 \\ \dot{\phi}_2 \\ z_1 \\ z_2 \end{bmatrix} = \begin{bmatrix} f_x(\underline{x}) \\ f_\phi(\underline{x}) \\ f_\delta(\underline{x}) \\ \dot{\phi}_1 \\ \dot{\phi}_2 \\ -\alpha_{p1}\dot{\theta}_1 + \beta_{p1}z_1 \\ -\alpha_{p2}\dot{\theta}_2 + \beta_{p2}z_2 \\ -\alpha_{s1}\dot{\phi}_1 \\ -\alpha_{s2}\dot{\phi}_2 \\ 0 \\ 0 \end{bmatrix} + \begin{bmatrix} 0 & 0 & 0 & 0 \\ 0 & 0 & 0 & 0 \\ 0 & 0 & 0 & 0 \\ 0 & 0 & 0 & 0 \\ 0 & 0 & 0 & 0 \\ 0 & 0 & 0 & 0 \\ 0 & 0 & 0 & 0 \\ 0 & 0 & \beta_{s1} & 0 \\ 0 & 0 & 0 & \beta_{s2} \\ 1 & 0 & 0 & 0 \\ 0 & 1 & 0 & 0 \end{bmatrix} \begin{bmatrix} w_1 \\ w_2 \\ w_3 \\ w_4 \end{bmatrix} \quad (6)$$

$$\underline{y} = \begin{bmatrix} x & \dot{y}_L & \phi & \delta \end{bmatrix}^T$$

where we define the enlarged state vector as  $\underline{x}_e = [x \ \phi \ \delta \ \phi_1 \ \phi_2 \ \dot{\theta}_1 \ \dot{\theta}_2 \ \dot{\phi}_1 \ \dot{\phi}_2 \ z_1 \ z_2]^T$ . Differentiating outputs  $x$ ,  $\phi$ , and  $\delta$  three times and output  $\dot{y}_L$  twice, we now obtain

$$\begin{bmatrix} \ddot{x} & \ddot{y}_L & \ddot{\phi} & \ddot{\delta} \end{bmatrix}^T = A_e(\underline{x}_e) + B_e(\underline{x}_e) \begin{bmatrix} w_1 & w_2 & w_3 & w_4 \end{bmatrix}^T \quad (7)$$

where  $A_e(\underline{x}_e)$  is a nonlinear vector and  $B_e(\underline{x}_e)$  is a nonlinear square matrix. By computing the inverse of  $B_e(\underline{x}_e)$ , it can be shown that this matrix is non-singular as long as the sheet is always moving in the process direction ( $\dot{\theta}_1, \dot{\theta}_2 \neq 0$ ). Thus, if we apply the feedback linearization control law

$$\begin{bmatrix} w_1 & w_2 & w_3 & w_4 \end{bmatrix}^T = B_e(\underline{x}_e)^{-1}(\underline{v}(\underline{x}_e) - A_e(\underline{x}_e))$$

$$\underline{v}(\underline{x}_e) = \begin{bmatrix} \ddot{x}_d + k_x(\ddot{x}_d - \ddot{x}) + l_x(\dot{x}_d - \dot{x}) + \lambda_x(x_d - x) \\ \ddot{y}_d + k_y(\ddot{y}_d - \ddot{y}) + l_y(\dot{y}_d - \dot{y}) \\ \ddot{\phi}_d + k_\phi(\ddot{\phi}_d - \ddot{\phi}) + l_\phi(\dot{\phi}_d - \dot{\phi}) + \lambda_\phi(\phi_d - \phi) \\ \ddot{\delta}_d + k_\delta(\ddot{\delta}_d - \ddot{\delta}) + l_\delta(\dot{\delta}_d - \dot{\delta}) + \lambda_\delta(\delta_d - \delta) \end{bmatrix} \quad (8)$$

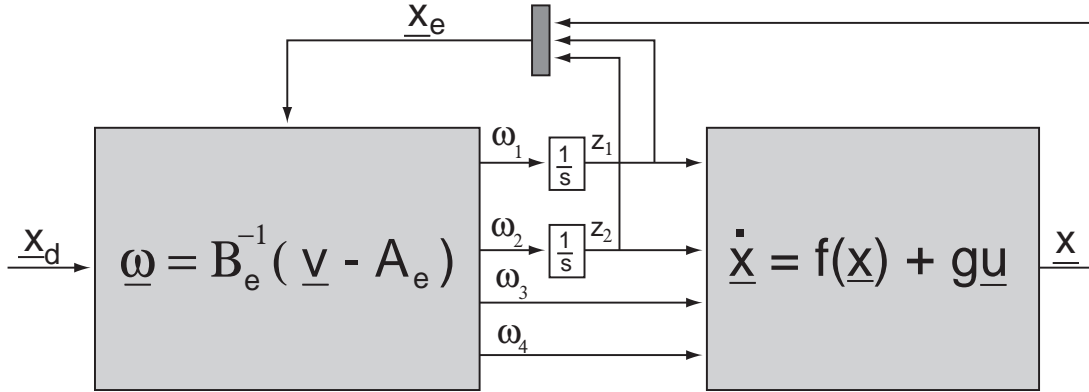


FIG. 3: Dynamic Feedback Linearization Controller

by proper selection of gains  $k$ 's,  $l$ 's, and  $\lambda$ 's through pole placement, we can guarantee that the state errors converge to zero. Furthermore, since the enlarged system consist of 11 states and the relative degree is also 11, there are no internal dynamics, and we can conclude that the enlarged system is exponentially stable. The block diagram for this control strategy is shown in Fig. 3. Using this control law, for a sheet moving at a nominal velocity of  $\nu = 0.5m/s$  and having initial errors  $(x(0), \dot{y}_L(0), \phi(0), \delta(0)) = (8mm, 30mm/s, 2.5mrad, 0.1mm)$  we obtain the simulation results shown in Fig. 4. The dashed line in Fig. 4 shows that the dynamic feedback linearization controller does a good job in reducing initial errors when we only consider a nominal plant for the actuators. However, this control strategy fails when we consider actuator multiplicative uncertainties as in Fig. 5, where  $P_{ji}$  is the actuator plant given by Eqs.(2), and  $\Delta_{ji}$  is the uncertainty dynamics given by

$$\Delta_{pi}(s) = \frac{\delta_{pi}}{(s+m_{pi})^2}; \quad \Delta_{si}(s) = \frac{\delta_{si}}{s+m_{si}}; \quad i = 1, 2 \quad (9)$$

In particular, the solid line in Fig. 4 shows the results when multiplicative uncertainty is introduced to the system with  $m_{pi} = m_{si} = 1.5$  and  $\delta_{pi} = \delta_{si} = 1$  for  $i = 1, 2$ . Here it is shown that the control strategy fails not only because it is not able to eliminate errors in the longitudinal velocity of the sheet, but also because it stretches the page (negative values for the error in buckling), which should never occur. In Section V we will compare the robustness of this control strategy to the one presented in the following section.

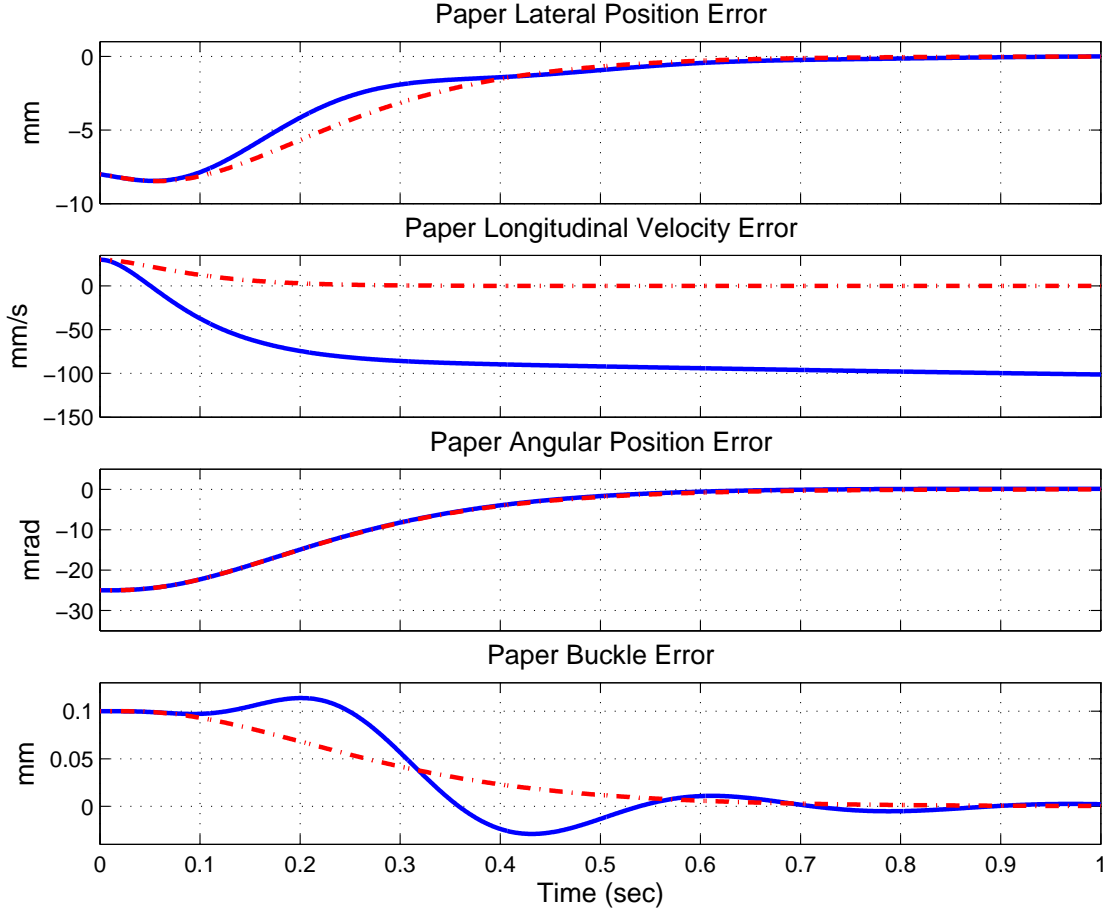


FIG. 4: Simulation results using the Dynamic Feedback Linearization controller. The solid and dashed lines represent the results with and without actuator multiplicative uncertainty, respectively.

#### IV. ROBUST FEEDBACK LINEARIZATION PLUS INNER LOOPS CONTROLLER

The control strategy presented in this section uses similar concepts to those described in Section III. However, instead of linearizing the whole system, we use feedback linearization only to linearize the kinematics, and use inner loops to locally control the actuator's rotational velocities and steering positions. Figure 6 shows the control strategy implemented to the real system. There, the feedback linearization controller,  $C_{FBL}$ , produces desired rotational accelerations and desired steering velocities, which after being integrated, are used as references to locally control the actuators, which are represented by blocks  $P_{ji}$  ( $j=p,s$ ;  $i=1,2$ ). It should be noticed that by feedback linearizing only the kinematics and not the dynamics of the system (as opposed to the controller presented in the previous section) the

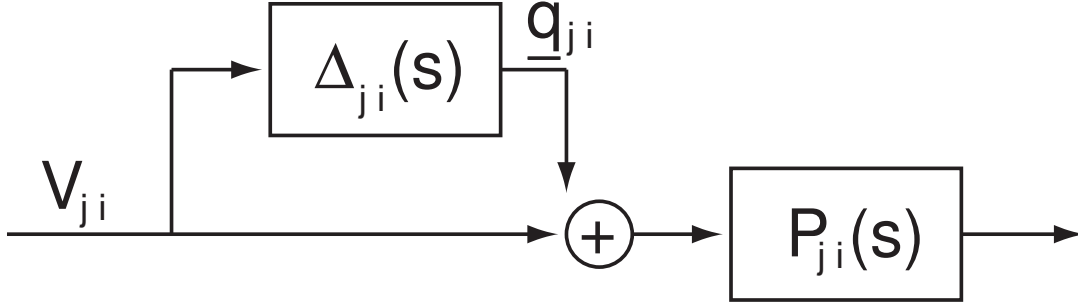


FIG. 5: Actuator multiplicative uncertainty ( $j = s, p, i = 1, 2$ )

control system gains in robustness since the local controllers can efficiently handle actuator uncertainties. This will be formally proven in Section V. The actuators in Fig. 6 are controlled through feedback plus feedforward; these local controllers are

$$\begin{aligned} C_{FB_{pi}}(s) &= \eta_{pi} + \frac{\gamma_{pi}}{s}; & C_{FF_{pi}} &= \frac{1}{\beta_{pi}} \left(1 + \frac{\alpha_{pi}}{s}\right) \\ C_{FB_{si}}(s) &= \eta_{si} + \gamma_{pi}s; & C_{FF_{pi}} &= \frac{1}{\beta_{si}} \left(1 + \frac{\alpha_{si}}{s}\right) \end{aligned} \quad (10)$$

where  $\eta$ 's and  $\gamma$ 's are controller gains,  $\alpha$ 's and  $\beta$ 's are the actuator coefficients defined in Eqs. (2) and subindex  $i$  corresponds to each of the two rollers. In order to be able to estimate the desired steering acceleration,  $\ddot{\phi}_{id}$  (needed for feedforward control), we use two first order filters, a technique called dynamic surface control and described in [14]. Note that if filter gain  $\tau_i$  is sufficiently small, the value of the signal generated by the controller  $C_{FBL}$ ,  $\dot{\phi}_i$ , will be very close to that of the filter output,  $\dot{\phi}_{id}$ . In order to obtain the feedback linearization law,  $C_{FBL}$ , we need to differentiate outputs  $x$ ,  $\phi$ , and  $\delta$  twice, and output  $\dot{y}_L$  once before the kinematics inputs appear, obtaining the expression

$$\begin{bmatrix} \ddot{x} & \ddot{y}_L & \ddot{\phi} & \ddot{\delta} \end{bmatrix}^T = A_r(\underline{x}) + B_r(\underline{x}) \begin{bmatrix} \ddot{\theta}_1 & \ddot{\theta}_2 & \dot{\phi}_1 & \dot{\phi}_2 \end{bmatrix}^T \quad (11)$$

where, again,  $A_r(\underline{x})$  is a nonlinear vector, and  $B_r(\underline{x})$  is a nonlinear square matrix. Note that by computing the inverse of  $B_r(\underline{x})$ , it can be shown that this matrix is invertible as long as the sheet is always moving along the process direction ( $\dot{\theta}_1, \dot{\theta}_2 \neq 0$ ). Thus, we can safely

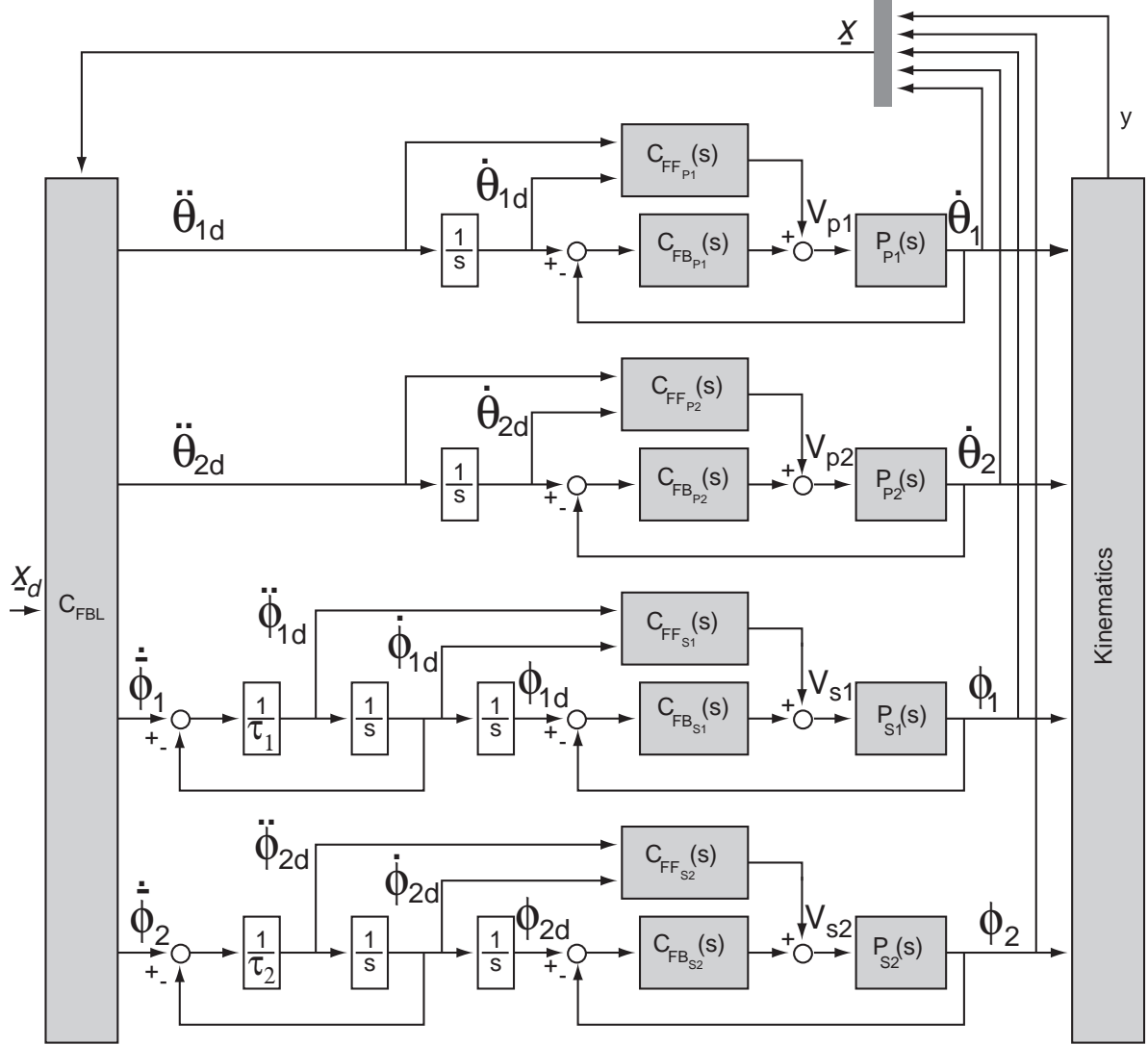


FIG. 6: Robust Feedback Linearization Plus Inner Loops Controller

apply the following feedback linearization law (block  $C_{FBL}$  in Fig.6):

$$\begin{bmatrix} \ddot{\theta}_{1d} & \ddot{\theta}_{2d} & \dot{\phi}_1 & \dot{\phi}_2 \end{bmatrix}^T = B_r(\underline{x})^{-1}(\underline{v}(\underline{x}) - A_r(\underline{x})) \quad (12)$$

$$\underline{v}(\underline{x}) = \begin{bmatrix} \ddot{x}_d + (k_x + \lambda_x)(\dot{x}_d - \dot{x}) + k_x \lambda_x (x_d - x) \\ \ddot{y}_d + k_y (\dot{y}_d - \dot{y}) \\ \ddot{\phi}_d + (k_\phi + \lambda_\phi)(\dot{\phi}_d - \dot{\phi}) + k_\phi \lambda_\phi (\phi_d - \phi) \\ \ddot{\delta}_d + (k_\delta + \lambda_\delta)(\dot{\delta}_d - \dot{\delta}) + k_\delta \lambda_\delta (\delta_d - \delta) \end{bmatrix} \quad (13)$$

where  $k$ 's and  $\lambda$ 's are controller gains. Fig. 7 shows simulation results for the controller just presented using the same initial conditions as those used for the control system described

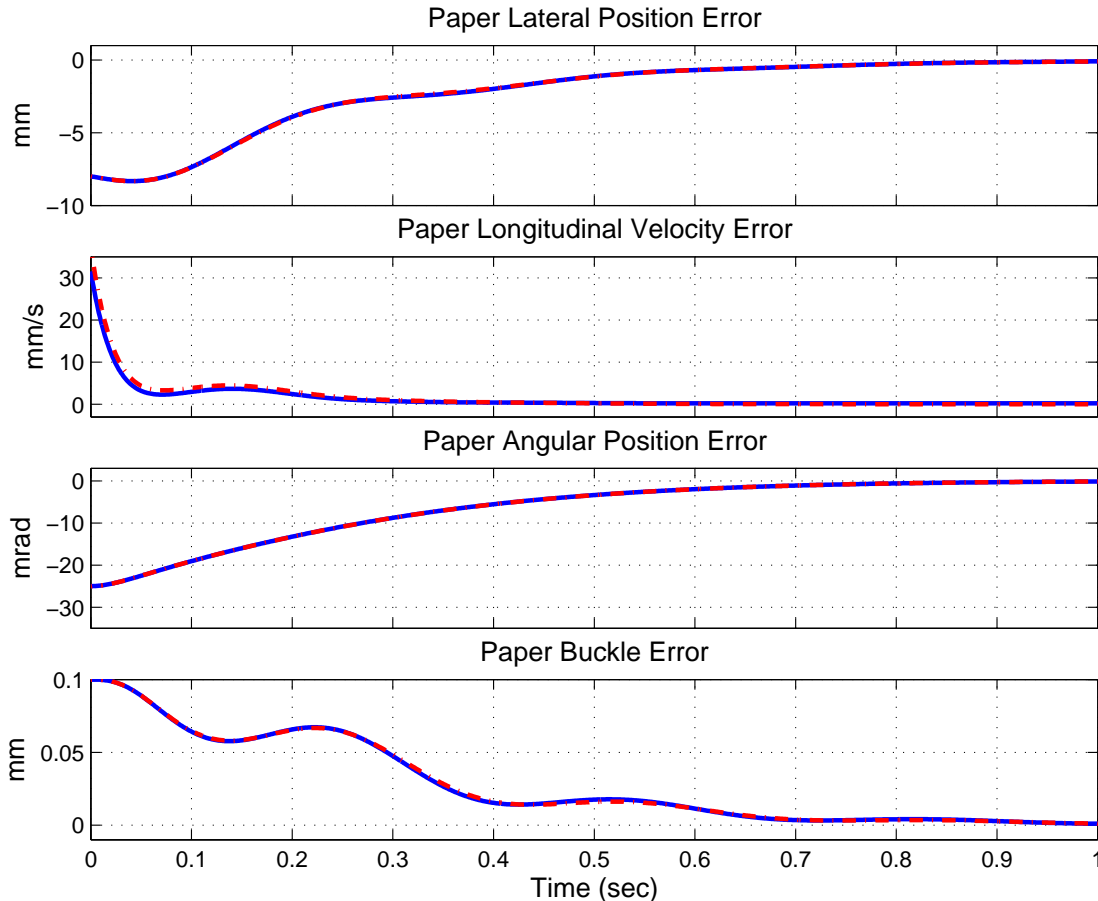


FIG. 7: Simulation results using the Robust Feedback Linearization Plus Inner Loops controller. Note that the results without uncertainty (dashed line) and those with uncertainty (solid line) are almost indistinguishable.

in Section III. This figure shows results for the cases with and without the multiplicative uncertainties defined in Eqs. (9). Contrary to the results obtained using the controller described in Section III, the *Robust Feedback Linearization Plus Inner Loops* controller corrects for the initial errors of the sheet in both cases. The exponential stability of the closed-loop system and its robustness to actuator multiplicative uncertainties will be proved in the next section.

## V. ROBUSTNESS ANALYSIS

In this section we will first show exponential stability of the *Robust Feedback Linearization Plus Inner Loops* nominal control through the indirect method of Lyapunov, and then we

will show its robustness to actuator multiplicative uncertainties. Finally, we will compare its robustness to that of the *Dynamic Feedback Linearization* control system presented in Section III.

### A. Stability of the Robust Feedback Linearization Plus Inner Loops Control Strategy

Let us first define paper coordinate and actuator errors by

$$\begin{aligned}\tilde{x} &= x_d - x; & \tilde{\phi} &= \phi_d - \phi \\ \tilde{\delta} &= \delta_d - \delta; & \epsilon_i &= \dot{\tilde{\phi}}_i - \dot{\phi}_{id}; \quad (i = 1, 2) \\ \epsilon_{pi} &= \dot{\theta}_{id} - \dot{\theta}_i; & \epsilon_{si} &= \phi_{id} - \phi_i; \quad (i = 1, 2)\end{aligned}\tag{14}$$

and let us also define the following surface errors:

$$\begin{aligned}s_x &= \dot{\tilde{x}} + \lambda_x \tilde{x}; & s_y &= \dot{\tilde{y}} = \dot{y}_d - \dot{y}_L \\ s_\phi &= \dot{\tilde{\phi}} + \lambda_\phi \tilde{\phi}; & s_\delta &= \dot{\tilde{\delta}} + \lambda_\delta \tilde{\delta} \\ s_{\epsilon_{p1}} &= \dot{\epsilon}_{p1} + \lambda_{\epsilon_{p1}} \epsilon_{p1}; & s_{\epsilon_{s1}} &= \dot{\epsilon}_{s1} + \lambda_{\epsilon_{s1}} \epsilon_{s1} \\ s_{\epsilon_{p2}} &= \dot{\epsilon}_{p2} + \lambda_{\epsilon_{p2}} \epsilon_{p2}; & s_{\epsilon_{s2}} &= \dot{\epsilon}_{s2} + \lambda_{\epsilon_{s2}} \epsilon_{s2}\end{aligned}\tag{15}$$

Combining Eqs. (11)-(14) we obtain the closed-loop expression

$$\begin{bmatrix} \ddot{x} & \dot{y}_L & \ddot{\phi} & \ddot{\delta} \end{bmatrix}^T = \underline{v}(\underline{x}) - A_r(\underline{x}) \begin{bmatrix} \dot{\epsilon}_{p1} & \dot{\epsilon}_{p2} & (\dot{\epsilon}_{s1} + \epsilon_1) & (\dot{\epsilon}_{s2} + \epsilon_2) \end{bmatrix}^T\tag{16}$$

If we further express  $\underline{v}(\underline{x})$  in terms of paper and surface errors and let the gains  $\gamma_{pi}$  and  $\eta_{si}$  ( $i = 1, 2$ ) in Eqs. (10) be equal to:

$$\begin{aligned}\gamma_{pi} &= \frac{(\alpha_{pi} + \beta_{pi} \eta_{pi} - \lambda_{\epsilon_{pi}}) \lambda_{\epsilon_{pi}}}{\beta_{pi}}; & (i = 1, 2) \\ \eta_{si} &= \frac{(\alpha_{si} + \gamma_{si} \beta_{si} - \lambda_{\epsilon_{si}}) \lambda_{\epsilon_{si}}}{\beta_{si}}; & (i = 1, 2)\end{aligned}\tag{17}$$

the time derivatives of the errors in Eqs. (14) and (15) are:

$$\begin{aligned}
\dot{\tilde{x}} &= -\lambda_x \tilde{x} + s_x \\
\dot{\tilde{\phi}} &= -\lambda_\phi \tilde{\phi} + s_\phi \\
\dot{\tilde{\delta}} &= -\lambda_\delta \tilde{\delta} + s_\delta \\
\dot{\varepsilon}_{p1} &= -\lambda_{p1} \varepsilon_{p1} + s_{\varepsilon_{p1}} \\
\dot{\varepsilon}_{p2} &= -\lambda_{p2} \varepsilon_{p2} + s_{\varepsilon_{p2}} \\
\dot{\varepsilon}_{s1} &= -\lambda_{s1} \varepsilon_{s1} + s_{\varepsilon_{s1}} \\
\dot{\varepsilon}_{s2} &= -\lambda_{s2} \varepsilon_{s2} + s_{\varepsilon_{s2}} \\
\dot{s}_x &= -K_x s_x + b_{11} \dot{\varepsilon}_{p1} + b_{12} \dot{\varepsilon}_{p2} + b_{13} \dot{\varepsilon}_{s1} + b_{14} \dot{\varepsilon}_{s2} \\
\dot{s}_y &= -K_y s_y + b_{21} \dot{\varepsilon}_{p1} + b_{22} \dot{\varepsilon}_{p2} + b_{23} \dot{\varepsilon}_{s1} + b_{24} \dot{\varepsilon}_{s2} \\
\dot{s}_\phi &= -K_\phi s_\phi + b_{31} \dot{\varepsilon}_{p1} + b_{32} \dot{\varepsilon}_{p2} + b_{33} \dot{\varepsilon}_{s1} + b_{34} \dot{\varepsilon}_{s2} \\
\dot{s}_\delta &= -K_\delta s_\delta + b_{41} \dot{\varepsilon}_{p1} + b_{42} \dot{\varepsilon}_{p2} + b_{43} \dot{\varepsilon}_{s1} + b_{44} \dot{\varepsilon}_{s2} \\
\dot{s}_{\varepsilon_{p1}} &= -(\alpha_{p1} + \beta_{p1} \eta_{p1} - \lambda_{\varepsilon_{p1}}) s_{\varepsilon_{p1}} \\
\dot{s}_{\varepsilon_{p2}} &= -(\alpha_{p2} + \beta_{p2} \eta_{p2} - \lambda_{\varepsilon_{p2}}) s_{\varepsilon_{p2}} \\
\dot{s}_{\varepsilon_{s1}} &= -(\alpha_{s1} + \beta_{s1} \eta_{s1} - \lambda_{\varepsilon_{s1}}) s_{\varepsilon_{s1}} \\
\dot{s}_{\varepsilon_{s2}} &= -(\alpha_{s2} + \beta_{s2} \eta_{s2} - \lambda_{\varepsilon_{s2}}) s_{\varepsilon_{s2}} \\
\dot{\epsilon}_1 &= -\frac{1}{\tau_1} \epsilon_1 + \frac{\partial \dot{\phi}_1}{\partial \underline{\Psi}} \underline{\dot{\Psi}} + \frac{\partial \dot{\phi}_1}{\partial t} \\
\dot{\epsilon}_2 &= -\frac{1}{\tau_2} \epsilon_2 + \frac{\partial \dot{\phi}_2}{\partial \underline{\Psi}} \underline{\dot{\Psi}} + \frac{\partial \dot{\phi}_2}{\partial t}
\end{aligned} \tag{18}$$

where  $b_{ij}$  is the  $(i, j)$ th element of matrix  $B_r(\underline{x})$  in Eq. (11), and  $\underline{\Psi}$  is defined by

$$\underline{\Psi} = \left[ \tilde{x} \ s_x \ s_y \ \tilde{\phi} \ s_\phi \ \tilde{\delta} \ s_\delta \right]^T \tag{19}$$

Eqs. (18) can be rewritten in compact form as

$$\dot{\underline{e}}(t) = f(\underline{e}(t)) \tag{20}$$

where the error vector  $\underline{e}(t)$  is given by

$$\underline{e}(t) = \left[ \bar{x} \quad \bar{y} \quad \bar{\phi} \quad \bar{\delta} \quad \bar{\varepsilon}_{p1} \quad \bar{\varepsilon}_{p2} \quad \bar{\varepsilon}_{s1} \quad \bar{\varepsilon}_{s2} \right]^T \quad (21)$$

and the elements of  $\underline{e}(t)$  are

$$\begin{aligned} \bar{x} &= \begin{bmatrix} \tilde{x} \\ s_x \end{bmatrix}; & \bar{y} &= s_y; & \bar{\phi} &= \begin{bmatrix} \tilde{\phi} \\ s_\phi \end{bmatrix}; & \bar{\delta} &= \begin{bmatrix} \tilde{\delta} \\ s_\delta \end{bmatrix} \\ \bar{\varepsilon}_{p1} &= \begin{bmatrix} \varepsilon_{p1} \\ s_{\varepsilon_{p1}} \end{bmatrix}; & \bar{\varepsilon}_{p2} &= \begin{bmatrix} \varepsilon_{p2} \\ s_{\varepsilon_{p2}} \end{bmatrix}; & \bar{\varepsilon}_{s1} &= \begin{bmatrix} \varepsilon_{s1} \\ s_{\varepsilon_{s1}} \end{bmatrix}; & \bar{\varepsilon}_{s2} &= \begin{bmatrix} \varepsilon_{s2} \\ s_{\varepsilon_{s2}} \end{bmatrix} \end{aligned} \quad (22)$$

If we now define the desired trajectory by  $(x_d, \phi_d, \delta_d, \dot{x}_d, \dot{y}_d, \dot{\phi}_d, \dot{\delta}_d) = (0, 0, 0, 0, \nu, 0, 0)$ , where  $\nu$  is the nominal longitudinal velocity of the sheet, and we linearize the system described in Eqs. (18) around  $\tilde{x} = \tilde{\phi} = \tilde{\delta} = \varepsilon_{p1} = \varepsilon_{p2} = \varepsilon_{s1} = \varepsilon_{s2} = s_x = s_y = s_\phi = s_\delta = s_{\varepsilon_{p1}} = s_{\varepsilon_{p2}} = s_{\varepsilon_{s1}} = s_{\varepsilon_{s2}} = \epsilon_1 = \epsilon_2 = 0$ , we can obtain an expression of the form

$$\dot{\underline{e}}(t) = G\underline{e}(t) \quad (23)$$

where  $G$  is given by

$$G = \begin{bmatrix} A_x & 0 & 0 & 0 & 0 & 0 & 0 & B_x^{\varepsilon_{s2}} & B_x^\epsilon \\ 0 & A_y & 0 & 0 & B_y^{\varepsilon_{p1}} & B_y^{\varepsilon_{p2}} & 0 & 0 & 0 \\ 0 & 0 & A_\phi & 0 & B_\phi^{\varepsilon_{p1}} & B_\phi^{\varepsilon_{p2}} & 0 & 0 & 0 \\ 0 & 0 & 0 & A_\delta & 0 & 0 & B_\delta^{\varepsilon_{s1}} & B_\delta^{\varepsilon_{s2}} & B_\delta^\epsilon \\ 0 & 0 & 0 & 0 & A_{\varepsilon_{p1}} & 0 & 0 & 0 & 0 \\ 0 & 0 & 0 & 0 & 0 & A_{\varepsilon_{p2}} & 0 & 0 & 0 \\ 0 & 0 & 0 & 0 & 0 & 0 & A_{\varepsilon_{s1}} & 0 & 0 \\ 0 & 0 & 0 & 0 & 0 & 0 & 0 & A_{\varepsilon_{s2}} & 0 \\ B_\epsilon^x & 0 & B_\epsilon^\phi & B_\epsilon^\delta & B_\epsilon^{\varepsilon_{p1}} & B_\epsilon^{\varepsilon_{p2}} & B_\epsilon^{\varepsilon_{s1}} & B_\epsilon^{\varepsilon_{s2}} & A_\epsilon \end{bmatrix} \quad (24)$$

where matrices  $A$ 's depend only on controller gains and matrices  $B$ 's depend on controller gains as well as on system parameters. We can then easily rearrange the elements in Eq.

(23) to obtain an expression of the form

$$\begin{bmatrix} \dot{n}_1 \\ \dot{n}_2 \end{bmatrix} = \begin{bmatrix} A_{n_1} & 0 \\ B_{n_2}^{n_1} & A_{n_2} \end{bmatrix} \begin{bmatrix} n_1 \\ n_2 \end{bmatrix} \quad (25)$$

and therefore, the solutions for  $n_1(t)$  and  $n_2(t)$  are given by

$$\begin{aligned} n_1(t) &= e^{A_{n_1}t} n_1(0) \\ n_2(t) &= e^{A_{n_2}t} n_2(0) + \left[ \int_0^t e^{A_{n_2}(t-\tau)} B_{n_2}^{n_1} e^{A_{n_1}\tau} d\tau \right] n_1(0) \end{aligned} \quad (26)$$

It is easy to show now that by proper selection of the controller gains ( $\lambda$ 's and  $k$ 's in Eq. (13) and  $\eta$ 's and  $\gamma$ 's in Eq. (10)), there exist positive constants  $\bar{k}$  and  $\bar{\gamma}$  such that

$$\|\underline{e}(t)\| \leq \bar{k} \|\underline{e}(0)\| \exp(-\bar{\gamma} t) \quad (27)$$

and therefore the linearized error dynamics in Eq. (23) are exponentially stable. Furthermore, if we define the Lyapunov function

$$v(\underline{e}) = \underline{e}^T P \underline{e} \quad (28)$$

where  $P$  is the positive definite solution to the Lyapunov equation

$$G^T P + P G = -Q \quad (29)$$

and  $Q$  is any positive definite matrix, we obtain the bounds

$$\lambda_{\min}(P) \|\underline{e}\|^2 \leq v(\underline{e}) \leq \lambda_{\max}(P) \|\underline{e}\|^2 \quad (30)$$

$$\dot{v}(\underline{e}) \leq -\lambda_{\min}(Q) \|\underline{e}\|^2 \quad (31)$$

$$\left\| \frac{\partial v}{\partial \underline{e}} \right\| \leq \lambda_{\max}(P) \|\underline{e}\| \quad (32)$$

It can further be shown that if we rewrite Eq. (20) as

$$\dot{\underline{e}} = G \underline{e}(t) + f_1(\underline{e}(t)) \quad (33)$$

where  $G$  is given by Eq. (24), and define the Lyapunov function as in Eq. (28), where  $P$  is given by Eq. (29), then  $v(\underline{e})$  satisfies inequalities (30) and (32). Moreover, since  $f_1(\underline{e})$  satisfies  $\lim_{\|\underline{e}\| \rightarrow 0} \frac{\|f_1(\underline{e})\|}{\|\underline{e}\|} = 0$ , then for any  $k > 0$ ,  $\exists r > 0$  such that  $\|f_1(\underline{e})\| \leq k\|\underline{e}\| \forall \|\underline{e}\| < r$ . In particular, if we let  $k = \alpha\lambda_{\min}(Q)/2\lambda_{\max}(P)$  with  $0 < \alpha < 1$ , then  $\exists r > 0$  such that, for all  $\|\underline{e}\| < r$ , we have

$$\dot{v}(\underline{e}) \leq -\lambda_{\min}(Q)(1 - \alpha)\|\underline{e}\|^2 \quad \text{with} \quad 0 < \alpha < 1 \quad (34)$$

and thus the nonlinear system in Eq. (20) is also locally exponentially stable.

### B. Robustness of the Robust Feedback Linearization Plus Inner Loops Control Strategy

Let us now analyze the robustness of the *Robust Feedback Linearization Plus Inner Loops* control strategy presented in Section IV to actuator multiplicative uncertainties. Specifically, when we consider the actuator uncertainties given by Eqs. (9) and shown in Fig. 5, the closed-loop system is given by

$$\dot{\underline{e}} = m(\underline{e}, \underline{q}) = f(\underline{e}(t)) - D\underline{q}(t) = G\underline{e}(t) + f_1(\underline{e}(t)) - D\underline{q}(t) \quad (35)$$

where  $f(\underline{e})$  is defined by Eq. (20),  $G$  and  $f_1(\underline{e}(t))$  by Eq. (33), the error state vector,  $\underline{e}(t)$ , is given by Eq. (21), the uncertainty state vector,  $\underline{q}(t)$ , is given by (see Fig. 5):

$$\underline{q}(t) = \left[ q_{p1}^1 \quad q_{p1}^2 \quad q_{p2}^1 \quad q_{p2}^2 \quad q_{s1} \quad q_{s2} \right]^T \quad (36)$$

and  $D$  is a constant matrix that depends only on actuator parameters  $\beta_{pi}$  and  $\beta_{si}$  ( $i = 1, 2$ ). Thus, we can put the system in the feedback form shown in Fig. 8, where system  $H_1$  is given by Eq. (35) with  $y_1 = [V_{p1} \quad V_{p2} \quad V_{s1} \quad V_{s2}]^T$ , and system  $H_2$  includes the uncertainty dynamics of all four actuators (Eqs. (9)) with  $y_2 = [q_{p1}^1 \quad q_{p2}^1 \quad q_{s1} \quad q_{s2}]^T$ . If we can now show that both

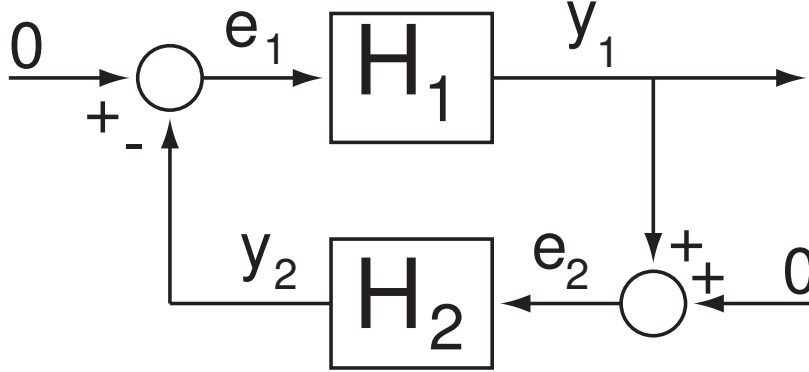


FIG. 8: Feedback connection for Small Gain Theorem

systems,  $H_i : \mathcal{L}_e^4 \rightarrow \mathcal{L}_e^4$ , are small-signal finite-gain  $\mathcal{L}_\infty$  stable:

$$\|y_{i\tau}\|_{L_\infty} \leq \gamma_i \|e_{i\tau}\|_{L_\infty} + \beta_i, \quad \forall e_i \in \mathcal{L}_e^4 \quad (37)$$

*with*  $\sup_{0 \leq t \leq \tau} \|e_i(t)\| \leq r_i$

for all  $\tau \in [0, \infty)$  (for  $i = 1, 2$ ), and also show that  $\gamma_1 \gamma_2 < 1$ , then by the Small Gain Theorem ([2] and [15]) we can conclude that the feedback connection in Fig. 8 is also small-signal finite-gain  $L_\infty$  stable, and therefore conclude robustness to actuator multiplicative uncertainties. Note that in Eq. (37) we needed to define mapping  $H_i$  in terms of extended spaces,  $\mathcal{L}_e$ , since input  $e_i \in \mathcal{L}^4$  may generate an output  $y_i$  that does not belong to  $\mathcal{L}^4$ . Moreover, we look at the truncation of functions up to time  $\tau$ :

$$f_\tau = \begin{cases} f(t), & 0 \leq t \leq \tau \\ 0, & \tau < t \end{cases} \quad (38)$$

In order to show small-signal finite-gain  $\mathcal{L}_\infty$  stability of systems  $H_1$  and  $H_2$ , we need to use the following theorem, which is presented in [15]:

**Theorem V.1** *Consider the system*

$$\begin{aligned} \dot{x} &= f(t, x, u); & x(0) &= x_o \\ y &= h(t, x, u) \end{aligned} \quad (39)$$

Let  $B_x = \{x \in \mathbb{R}^n \mid \|x\| < r\}$ ,  $B_u = \{u \in \mathbb{R}^m \mid \|u\| < r_u\}$ ,  $f : [0, \infty) \times B_x \times B_u \rightarrow \mathbb{R}^n$  be piecewise continuous in  $t$  and locally Lipschitz in  $(x, u)$ , and  $h : [0, \infty) \times B_x \times B_u \rightarrow \mathbb{R}^q$  be piecewise continuous in  $t$  and continuous in  $(x, u)$ . Suppose that:

(1)  $x = 0$  is an exponentially stable equilibrium point of  $\dot{x} = f(t, x, 0)$  and there is a Lyapunov function  $v(t, x)$  that satisfies

$$\begin{aligned} c_1 \|x\|^2 &\leq v(t, x) \leq c_2 \|x\|^2 \\ \dot{v}(t, x) &\leq -c_3 \|x\|^2 \\ \left\| \frac{\partial v}{\partial x} \right\| &\leq c_4 \|x\| \end{aligned} \tag{40}$$

for all  $(x, t) \in [0, \infty) \times B_x$  for some positive constants  $c_1$ - $c_4$ ;

(2)  $f$  and  $h$  satisfy the inequalities

$$\|f(t, x, u) - f(t, x, 0)\| \leq L \|u\| \tag{41}$$

$$\|h(t, x, u)\| \leq \eta_1 \|x\| + \eta_2 \|u\| \tag{42}$$

for all  $(t, x, u) \in [0, \infty) \times B_x \times B_u$  for some nonnegative constants  $L$ ,  $\eta_1$ , and  $\eta_2$ . Then, for each  $x_o$  with  $\|x_o\| < r\sqrt{c_1/c_2}$ , system in Eq. (39) is small-signal finite-gain  $\mathcal{L}_\infty$  stable. In particular, for each  $u \in \mathcal{L}_\infty$  with  $\sup_{0 \leq t \leq \tau} \|u(t)\| < \min\{r_u, c_1 c_3 r / c_2 c_4 L\}$ , the output  $y(t)$  satisfies

$$\|y_\tau\|_{\mathcal{L}_\infty} \leq \gamma \|u_\tau\|_{\mathcal{L}_\infty} + \beta, \quad \forall \tau \in [0, \infty) \tag{43}$$

$$\gamma = \eta_2 + \frac{\eta_1 c_2 c_4 L}{c_1 c_3}; \quad \beta = \eta_1 \|x_o\| \sqrt{c_2 / c_1} \tag{44}$$

The proof of this Theorem can be found in [15]. For our particular application, in order to show small-signal finite-gain  $\mathcal{L}_\infty$  stability of system  $H_1$ , let us first notice that in Section VA we have shown that  $\underline{e} = 0$  is an exponential equilibrium point of system  $\dot{\underline{e}} = m(\underline{e}, 0)$ . Also, by defining the Lyapunov function,  $v(\underline{e})$ , as in Eq. (28), we obtain the bounds  $c_1$ ,  $c_2$  and  $c_4$  for  $v(\underline{e})$  given by Eqs. (30) and (32), and  $\exists r > 0$  such that for all  $\|\underline{e}\| < r$ , bound  $c_3$  for  $\dot{v}(\underline{e})$  is given by Eq. (34). Furthermore, by looking at Eqs. (35) and (41) we have

$$\|m(\underline{e}, \underline{q}) - m(\underline{e}, 0)\| = \|G\underline{q}\| \leq \sigma_{max}(G) \|\underline{q}\| \tag{45}$$

Then, after obtaining  $\eta_1$  and  $\eta_2$  to satisfy the inequality in Eq. (42), we invoke Theorem

V.1 to conclude that system  $H_1$  is small-signal finite-gain  $\mathcal{L}_\infty$  stable and satisfies Eq. (37) with  $\gamma_1$  and  $\beta_1$  given by:

$$\begin{aligned}\gamma_1 &= \eta_2 + \frac{\eta_1 \sigma_{max}(D) \lambda_{max}^2(P)}{\lambda_{min}(P) \lambda_{min}(Q) (1-\alpha)} \\ \beta_1 &= \eta_1 \|\underline{e}(0)\| \sqrt{\lambda_{max}(P) / \lambda_{min}(P)}\end{aligned}\tag{46}$$

with  $0 < \alpha < 1$ . It is clear that the selection of matrix  $Q$  in Eq. (29) directly affects the value of  $\gamma_1$  in Eq. (46). Thus, in order to obtain a small value for  $\gamma_1$ , let  $T$  be composed by the eigenvectors (and generalized eigenvectors) corresponding to the eigenvalues of matrix  $G$ , and perform the similarity transformation  $\underline{e} = T\bar{\underline{e}}$ . We then obtain the following system equations:

$$\begin{aligned}\frac{d\bar{\underline{e}}}{dt} &= T^{-1}GT\bar{\underline{e}} + T^{-1}f_1(T\bar{\underline{e}}) - T^{-1}D\underline{q} = \bar{G}\bar{\underline{e}} + \bar{f}_1(\bar{\underline{e}}) - \bar{D}\underline{q} \\ y_1 &= \underline{u}(T\bar{\underline{e}})\end{aligned}\tag{47}$$

As with the original realization of system  $H_1$ , it can be shown that  $\exists r > 0$  such that for all  $\|\bar{\underline{e}}\| < r$  the inequality in Eq. (37) is satisfied with  $\gamma_1$  and  $\beta_1$  given by

$$\begin{aligned}\gamma_1 &= \eta_2 + \frac{\eta_1 \sigma_{max}(T) \sigma_{max}(T^{-1}G) \lambda_{max}^2(\bar{P})}{\lambda_{min}(\bar{P}) \lambda_{min}(\bar{Q}) (1-\alpha)} \\ \beta_1 &= \eta_1 \sigma_{max}(T) \|T\underline{e}(0)\| \sqrt{\lambda_{max}(\bar{P}) / \lambda_{min}(\bar{P})}\end{aligned}\tag{48}$$

with  $0 < \alpha < 1$ , where  $\bar{P}$  and  $\bar{Q}$  satisfy the Lyapunov equation

$$\bar{G}^T \bar{P} + \bar{P} \bar{G} = -\bar{Q}\tag{49}$$

with  $\bar{P} = T^T P T$  and  $\bar{Q} = T^T Q T$ . This time, however, since matrix  $\bar{G}$  is in Jordan form, we can select matrix  $\bar{Q}$  so that the ratio  $\lambda_{max}^2(\bar{P}) / \lambda_{min}(\bar{P}) \lambda_{min}(\bar{Q})$  in  $\gamma_1$  (Eq. (48)) is small.

We can similarly show that system  $H_2$  in Fig. 8 is small-signal finite-gain  $\mathcal{L}_\infty$  stable and obtain gains  $\gamma_2$  and  $\beta_2$ . Now, by using the controller gains used to obtain the simulation results shown in Fig. 7, we obtain the values for  $\gamma_i$  and  $\beta_i$  ( $i = 1, 2$ ) shown in Table I. Thus, since  $\gamma_1 \gamma_2 < 1$ , we conclude from the Small Gain Theorem that the feedback connection in Fig. 8 is small-signal finite-gain  $L_\infty$  stable, and therefore that the control system is robust to actuator multiplicative uncertainties.

RFLPIL Controller	DFL Controller
$\gamma_1 = 3.04$	$\gamma_1 = 762.04$
$\beta_1 = 1.05$	$\beta_1 = 0.36$
$\gamma_2 = 0.27$	$\gamma_2 = 0.16$
$\beta_2 = 0.002$	$\beta_2 = 0.003$

TABLE I: Gains required to show small-signal finite-gain  $\mathcal{L}_\infty$  stability of systems  $H_1$  and  $H_2$  for the *Robust Feedback Linearization Plus Inner Loops (RFLPIL)* Controller and the *Dynamic Feedback Linearization (DFL)* Controller

### C. Robustness of the Dynamic Feedback Linearization Control Strategy

For the case of the *Dynamic Feedback Linearization* controller described in Section III, we can perform a similar analysis. First, we obtain the error dynamics

$$\dot{\tilde{\mathbf{x}}}_e = \bar{m}(\tilde{\mathbf{x}}_e, q) = f(\tilde{\mathbf{x}}_e) - D\underline{q}(t) \quad (50)$$

where  $\tilde{\mathbf{x}}_e$  is the error state vector,  $f(\tilde{\mathbf{x}}_e)$  is obtained by combining Eqs. (6), (8), and (9);  $D$  and  $\underline{q}(t)$  are defined exactly as in Eq. (35). After linearizing  $\dot{\tilde{\mathbf{x}}}_e = f(\tilde{\mathbf{x}}_e)$  along  $\tilde{\mathbf{x}}_e = 0$ , we can put the system in the form of Fig. 8. We then show exponential stability of  $\tilde{\mathbf{x}}_e = 0$  and obtain constants  $c_1$ - $c_4$  as in Eqs. (30), (32) and (34). Once  $L$ ,  $\eta_1$ , and  $\eta_2$  are obtained as in the previous section, we use Eq. (48) to compute gains  $\gamma_1$  and  $\beta_1$ . Gains  $\gamma_2$  and  $\beta_2$  for system  $H_2$  in Fig. 8 are similarly obtained. Then, using the same controller gains as those used to obtain the results shown in Fig. 4, we obtain the values for  $\gamma_i$  and  $\beta_i$  ( $i = 1, 2$ ) shown in Table I. As seen in this table, this time  $\gamma_1\gamma_2 > 1$ , and thus we cannot conclude anything from the Small Gain Theorem; however, such a large value for  $\gamma_1$  indicates that the system may not be robust to actuator multiplicative uncertainties.

## VI. EXPERIMENTAL RESULTS

The conclusions just made regarding the robustness of the two control strategies presented are justified not only by the simulation results shown in Figs. 4 and 7, but also through experimental tests. Figure 9 shows experimental results when a sheet of finite length was introduced to the steerable nips section and we used the *Robust Feedback Linearization Plus Inner Loops* controller described in Section IV. Here, the lateral and longitudinal position of the page is defined by the position of the leading right corner of the page (point  $C$  in

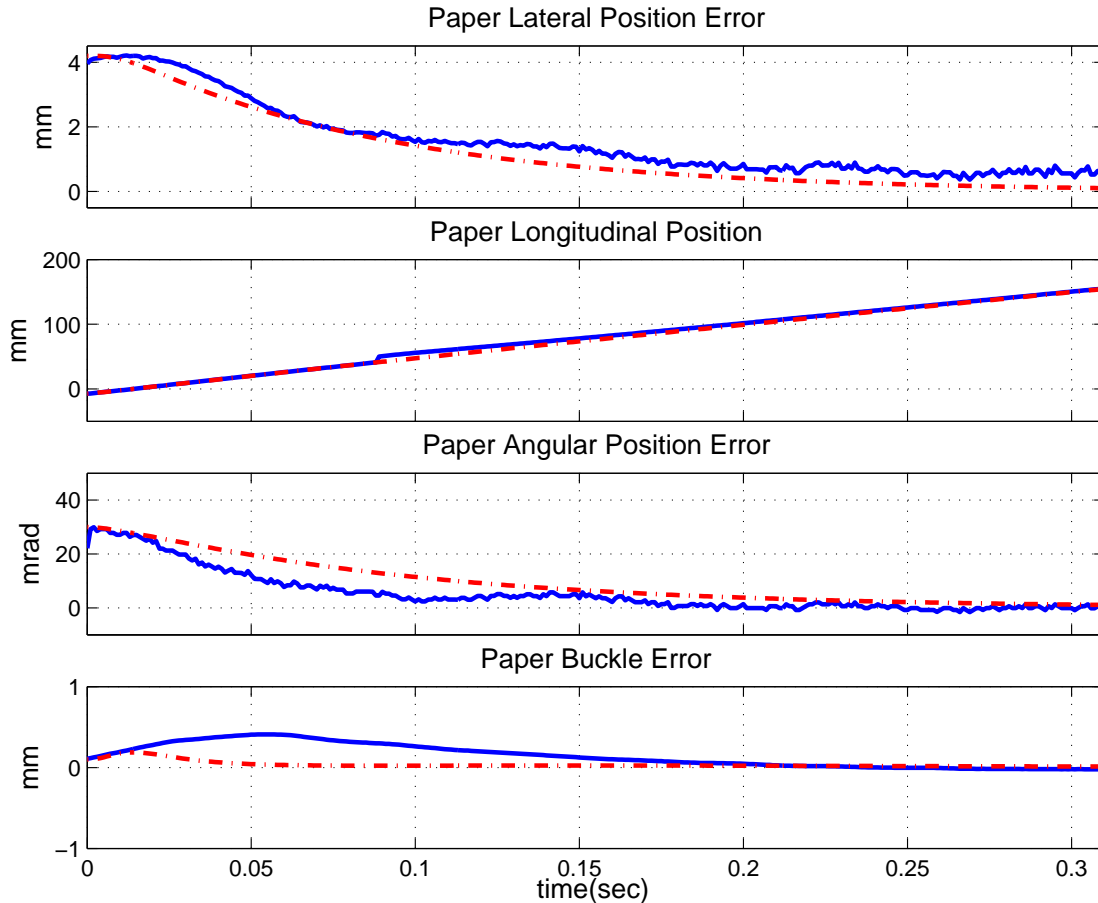


FIG. 9: Experimental results using the Robust Feedback Linearization Plus Inner Loops controller. The solid line is used for experimental results and the dashed line for simulation results.

Fig. 1). Figure 9 shows that we were able to correct the sheet’s position in about 0.3 seconds. Note that the longitudinal position increases steadily because the sheet moves in the longitudinal direction at all times. The small discrepancies observed between simulation and experimental results can be attributed to sensor noise and un-modeled dynamics.

When the *Dynamic Feedback Linearization* controller presented in Section III was tested on the experimental setup, it went unstable very quickly, and we were not able to collect any data because we did not want to risk the safety of our setup. However, in order to illustrate this instability, we performed a hybrid experiment, in which the real actuators were used, but we simulated the sheet by using the kinematic model. Those results are presented in Fig. 10, showing that this controller is not able to correct for the sheet initial position errors.

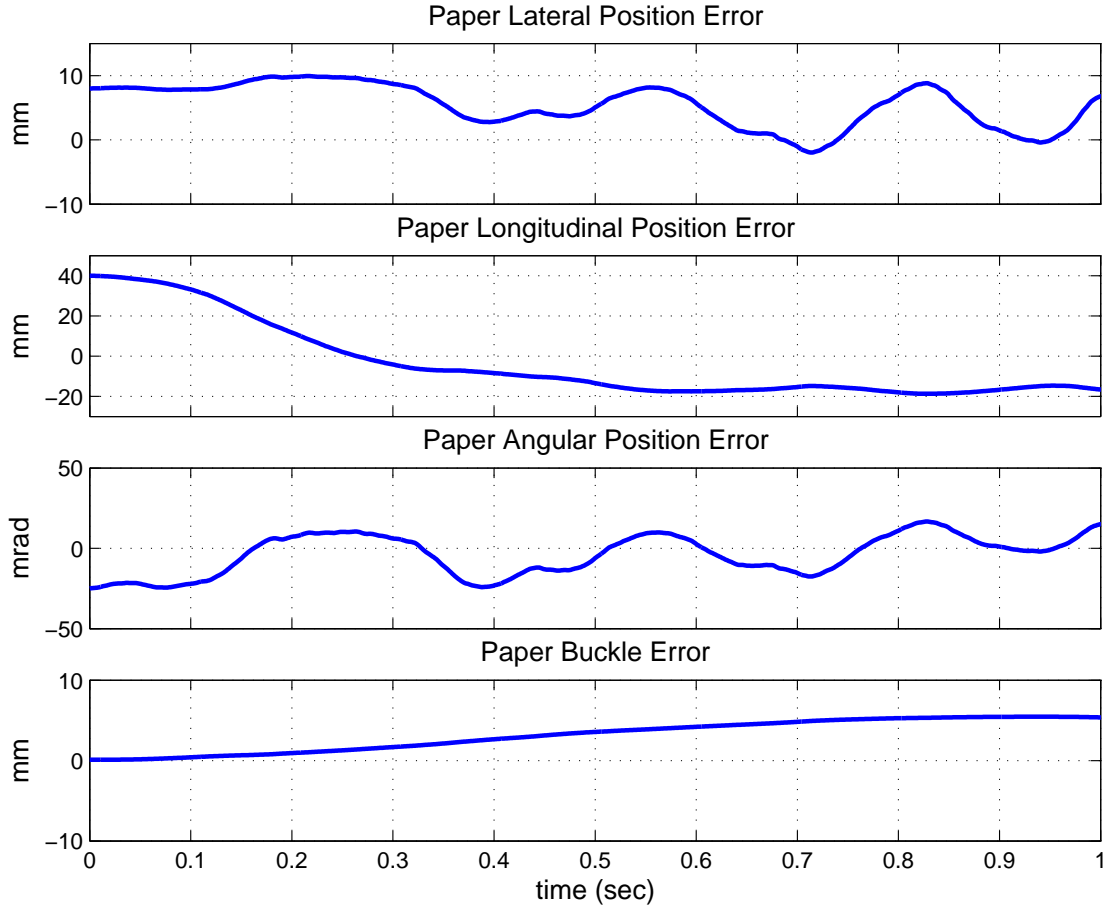


FIG. 10: Hybrid experimental results using the Dynamic Feedback Linearization controller, where real actuators were used, but the sheet response was simulated using the kinematic model.

## VII. CONCLUSION

In this paper we have shown the drawbacks of using a controller simply based on *Dynamic Feedback Linearization* due to un-modeled dynamics. Furthermore, we presented a robust modified version, which we call *Robust Feedback Linearization Plus Inner Loops* controller. Not only we proved that this control strategy is more robust to multiplicative uncertainties, but we also showed its successful implementation. This control strategy separates kinematics from actuator dynamics and uses feedback linearization only in the kinematics part of the system. Then we use internal loops to locally control the rotational velocity and steering position of the rollers through standard dynamic linear controllers. Besides simulation and experimental results, we have also presented a formal proof that corroborates our findings.

## VIII. ACKNOWLEDGEMENTS

This work was supported by the National Science Foundation under Grant CMS 0301719 and by Xerox Corporation.

- 
- [1] Alberto Isidori. *Nonlinear Control Systems*. Springer, 3rd edition, 1995.
  - [2] S. Shankar Sastry. *Nonlinear Systems : Analysis, Stability, and Control*. Springer, 1999.
  - [3] J. Descusse and C.H. Moog. Decoupling with dynamic compensation for strong invertible affine non-linear systems. *International Journal of Control*, 42(6):1287–1398, 1985.
  - [4] B. d’Andrea Novel, G. Campion, and G. Bastin. Control of nonholonomic wheeled mobile robots by state feedback linearization. *The International Journal of Robotics Research*, 14:543–559, 1995.
  - [5] Edgar Ergueta, Rene Sanchez, Roberto Horowitz, and Masayoshi Tomizuka. Convergence analysis of a steerable nips mechanism for full sheet control in printing devices. In *Journal of Dynamics Systems, Measurement and Control (Accepted for Publication)*, 2008.
  - [6] Edgar Ergueta. *Full Sheet Control Through the Use of a Steerable Nips Mechanism*. Ph.D. Thesis, University of California, Berkeley, 2008.
  - [7] Rene Sanchez, Roberto Horowitz, and Masayoshi Tomizuka. Paper sheet control using steerable nips. In *2004 American Control Conference Proceedings*, pages 482–487, Boston, Massachusetts, June 30–July 2 2004.
  - [8] Rene Sanchez, Edgar Ergueta, Benjamin Fine, Roberto Horowitz, Masayoshi Tomizuka, and Martin Krucinskić. A mechatronic approach to full sheet control using steerable nips. In *4th IFAC Symposium in Mechatronic Systems*, Heidelberg, Germany, September 12–15 2006.
  - [9] Rene Sanchez. *Nonlinear Control Strategies for a Steerable Nips Mechanism*. Ph.D. Thesis, University of California, Berkeley, 2006.
  - [10] Shyshung S Hwang et al. Sheet registration and deskewing system with independent drives and steering. United States Patent Number 6,634,521, August 2002.
  - [11] Xiaoping Yun and N. Sarkar. Dynamic feedback control of vehicles with two steerable wheels. In *1996 IEEE International Conference on Robotics and Automation*, pages 3105–3110, 1996.
  - [12] Edgar Ergueta, Robert Seifried, Roberto Horowitz, and Masayoshi Tomizuka. Extended Luen-

- berger Observer for a MIMO Nonlinear Nonholonomic System. In *17th IFAC World Congress*, Seoul, Korea, July 6–11 2008.
- [13] Edgar Ergueta, Rene Sanchez, Roberto Horowitz, and Masayoshi Tomizuka. A mechatronic approach to full sheet control using steer-able nips. In *ASME International Mechanical Engineering Congress and Exposition*, Seattle, Washington, November 11–15 2007.
- [14] D. Swaroop, J. C. Gerdes, P. P. Yip, and J. K. Hedrick. Dynamic Surface Control of Nonlinear Systems. In *Proceedings of the American Control Conference*, Albuquerque, New Mexico, pages 3028–3034, June 1997.
- [15] Hassan K. Khalil. *Nonlinear Systems*. Prentice Hall, Inc., 2nd edition, 1996.

## List of Figure Captions

- 1 Steerable nips with paper buckle.
- 2 Top view of steerable nips.
- 3 Dynamic Feedback Linearization Controller.
- 4 Simulation results using the Dynamic Feedback Linearization controller. The solid and dashed lines represent the results with and without actuator multiplicative uncertainty, respectively.
- 5 Actuator multiplicative uncertainty ( $j = s, p, i = 1, 2$ ).
- 6 Robust Feedback Linearization Plus Inner Loops Controller.
- 7 Simulation results using the Robust Feedback Linearization Plus Inner Loops controller. Note that the results without uncertainty (dashed line) and those with uncertainty (solid line) are almost indistinguishable.
- 8 Feedback connection for Small Gain Theorem.
- 9 Experimental results using the Robust Feedback Linearization Plus Inner Loops controller. The solid line is used for experimental results and the dashed line for simulation results.
- 10 Hybrid experimental results using the Dynamic Feedback Linearization controller, where real actuators were used, but the sheet response was simulated using the kinematic model.

## List of Table Captions

- I Gains required to show small-signal finite-gain  $\mathcal{L}_\infty$  stability of systems  $H_1$  and  $H_2$  for the *Robust Feedback Linearization Plus Inner Loops (RFLPIL)* Controller and the *Dynamic Feedback Linearization (DFL)* Controller.